Helical Encapsulation of Graphene Nanoribbon into Carbon Nanotube

Yanyan Jiang,[†] Hui Li,[†,*] Yunfang Li,[†] Haiqing Yu,[†] Kim M. Liew,[‡] Yezeng He,[†] and Xiangfa Liu[†]

[†]Key Laboratory for Liquid—Solid Structural Evolution and Processing of Materials, Ministry of Education, Shandong University, Jinan 250061, People's Republic of China and [‡]Department of Building and Construction, City University of Hong Kong, Kowloon, Hong Kong

ABSTRACT Molecular dynamics (MD) simulations were performed to study interaction between the graphene nanoribbon (GNR) and single-wall carbon nanotube (SWCNT). The GNR enters the SWCNT spontaneously to display a helical configuration which is quite similar to the chloroplast in the spirogyra cell. This unique phenomenon results from the combined action of the van der Waals potential well and the $\pi-\pi$ stacking interaction. The size of SWCNT and GNR should satisfy some certain conditions in the helical encapsulation process. A DNA-like double helix would be formed inside the SWCNT with the encapsulation of two GNRs. A water cluster enclosed in the SWCNT has great effect on the formation of the GNR helix in the tube. Furthermore, we also studied the possibility that the spontaneous encapsulation of GNR is used for substance delivery. The expected outcome of these properties is to provide novel strategies to design nanoscale carriers and reaction devices.

KEYWORDS: molecular dynamics simulation · graphene nanoribbon · carbon nanotube · helical configuration · the $\pi-\pi$ stacking interaction · nanoscale carriers

Carbon-based materials with a perfect honeycomb lattice, especially nanotubes, C_{60}, and carbon graphene, have attracted considerable attention on the theoretical research and the potential applications in materials science owing to their exotic properties. In the past 20 years, SWCNTs have elicited great research interest not only due to their unusual electrical[1] and mechanical properties[2] but also because their hollow interior[3] can serve as a nanosized container or template[4] in material fabrication. On one hand, the presence of encapsulated nanostructures in SWCNTs is known to alter the properties of the tube; on the other hand, since the particular one-dimensional advantages and the nanoscale structures make the fillers possess novel properties which are quite different from those of their bulk counterparts, filling SWCNTs with chosen materials can lead to nanostructures with exciting new applications. Moreover, the carbon shell is regarded as a natural protective layer of the fillers against oxidation.[5] The encapsulation of a wide array of materials, including metals, liquids, and fullerenes, within SWCNTs, and the properties of the fillers have been discussed both theoretically and experimentally. It has been acknowledged that metal nanoparticles enclosed in SWCNTs[6,7] have a lower melting point than the bulk metal[8] and can significantly enhance the mechanical properties of SWCNTs.[9] Water molecules confined in nanotubes usually have different transport behaviors from those of a bulk system.[10−13] Bai *et al.*[14] reported that the scale of the confinement may cause ice within the SWCNT to have different morphologies with bulk ice. Some theoretical studies[15,16] have addressed that DNA could be encapsulated inside the SWCNT in a water solute environment spontaneously because the van der Waals force as well as the hydrophobic force plays an indispensable role in the insertion course. More recently, Wang *et al.*[17] have synthesized a stable mixed low-dimensional nanomaterial consisting of MoS_2 inorganic nanoribbons encapsulated in carbon nanotube. As for another important carbon material C_{60}, Okada *et al.*[18] reported that the C_{60}@SWCNT (10,10) is a metal with multicarriers each of which distributes either along the nanotube or on the C_{60} chain. Jamie *et al.*[19] demonstrated that whenY@C82 metallofullerenes are inserted into SWCNTs with large diameters of 2 nm, the minimum energy configuration is a double-helix chiral structure extending over hundreds of nanometers. They also explained that rotation of the double-helix fullerene chain within the nanotube induces real time elastic distortions of the nanotube in a crank-shaft manner.

Although there have been large quantities of important discoveries on the encapsulation of various materials, including C_{60}, into SWCNTs, research on the encapsulation of graphene, a newly found carbon material with a honeycomb lattice, into the SWCNT is still missing. Graphene, the one-atom-thick

*Address correspondence to lihuilmy@hotmail.com.

Received for review December 5, 2010 and accepted January 27, 2011.

Published online February 10, 2011
10.1021/nn103317u

two-dimensional layer, shows fascinating physical properties.[20−23] Tailored from this 2D graphene sheet with finite width, GNRs are obviously more suitable to be inserted into the hollow tube due to their high aspect ratio. GNRs possess intriguing electronic structures ranging from semiconducting to half-metallic, depending on their geometry and dimensions.[24−29] Recently, an increasing number of researchers have paid their attention to the applications of GNRs in biochemical and medical realms.[30,31] A convincing model on the interaction between the GNR and SWCNT may inspire great efforts in theoretical studies, synthesis, and chemical modifications which focus on their electronic, biological, chemical and even magnetic properties.[32] All these properties depend greatly on the geometrical structure of the carbon materials especially the GNRs. Hence, what concerns us is how the GNR enters the SWCNT and what is the shape of the GNR inside the SWCNT. In this work we have carried out systematic theoretical investigations on the GNR−SWCNT interaction, which is essential to the substantial potential applications for exploring new theories and functional devices.

RESULTS AND DISCUSSION

Direct simulations in Figure 1 (see Video 1 in Supporting Information for detailed encapsulation process) provide the encapsulation of the GNR into the SWCNT and the evolution process. Initially, the GNR is placed along the axial direction of the SWCNT and the GNR end is inserted a little bit into the SWCNT in order to overcome the deformation force from the GNR itself. As shown in Figure 1, the GNR is too thin to keep thermodynamically unstable, becoming discontinuous wrinkles or corrugations at thicknesses of several nanometers, which is similar to the result of Bets[32] that at room temperature twists or bends arise in the GNR. According to the Mermin−Wagner theorem, long-wavelength fluctuations destroy the long-range order of 2D crystals. 2D graphene layers embedded in a 3D space have a tendency to be crumpled. These fluctuations can be suppressed by anharmonic coupling between the bending and stretching modes, meaning that a 2D membrane can exist but will exhibit strong ripples and corrugations.[33] The corrugations are intrinsic to graphene membranes. Theoretical investigations of 2D membranes have predicted their thermodynamic stability through static microscopic crumpling involving either bending or buckling. When the simulation continues, the GNR starts to enter the SWCNT gradually in a straight line. It is worth noting that the wrinkle of the GNR vanishes, which inspires us to explore the use of this performance to straighten some twisted and corrugated GNRs effectively.

When the simulation time is up to 6 ns, the GNR displays a clear helical conformation in the SWCNT. We would like to ask why the GNR gets in the SWCNT and takes on a helical shape when it fills the confining space. It must be pointed out that two interaction effects exist between the GNR and SWCNT during the encapsulation of the GNR into the SWCNT. One interaction results from the so-called van der Waals potential well in the SWCNT,[15] which makes the GNRs be trapped inside the tube; the other one is the offset face-to-face $\pi-\pi$ stacking interaction[34] which is an intermolecular interaction in the paralleled six-membered rings, that causes the GNR to be held tightly against the inner wall of the tube. There are two kinds of subinteractions existing in the offset face-to-face $\pi-\pi$ stacking interaction in the GNR−SWCNT: $\pi-\pi$ electron interaction and $\pi-\sigma$ interaction. The $\pi-\pi$ electron interaction is an important repulsive force, which is roughly proportional to the area of π-overlap of the two six-membered rings. Certainly, displacement of the interaction system diminishes the repulsion. The $\pi-\sigma$ interaction is an attractive force between π electrons of one ring and the σ-framework around the inner edge of the cavity of the other one. Different from $\pi-\pi$ electron interaction, this attractive interaction can be maximized in displaced stacking. Furthermore, in a stacking system, stacked molecules should be exactly parallel to reduce the π-system repulsion. Therefore, the best way to keep the displaced stacking and perfect parallel in the GNR−SWCNT system is that the arrangement of the GNR follows a helical mode around the inner wall of the SWCNT when increasingly longer GNR is trapped in the SWCNT. In helix, paralleled arrangements of six-membered system, displacement of the rings favors minimization of repulsive $\pi-\pi$ interaction and maximization of attractive interaction. To some extent, the flexibility of the GNR has also contributed to the formation of the GNR helix during the encapsulation process. In addition, the offset face-to-face $\pi-\pi$ stacking interaction and the flexibility of the GNR should also be responsible for the GNR's straight encapsulation before the helix happens. The experimental result of Snir and Kamien[35] is very valuable for better understanding this question. Snir and Kamien constructed the system as a flexible, unbreakable solid tube immersed in a solution of mixture of hard spheres. They found that the best configuration of the short flexible tube that takes the least mount of energy and takes up the least space is a helix with a geometric structure close to the helices found in nature. We suggest that helical filling of the GNR into the space of the SWCNT are perhaps because they are natural space savers and taking the least amount of energy.

The $\pi-\pi$ stacking interaction between GNR and SWCNT along the radial direction, of course, does not affect its moving freely along the axial and circumferential directions. When the simulation goes on, the front helical structure is pushed ahead of the ribbon outside the tube which continues to enter the SWCNT

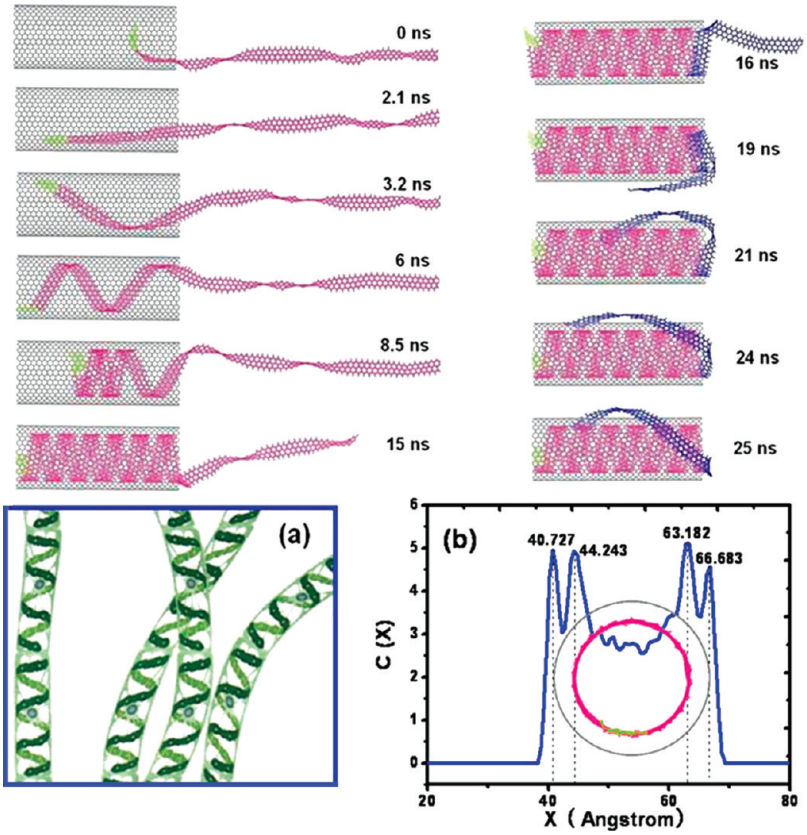

Figure 1. Snapshots of the insertion and helix-forming process of the GNR into the SWCNT. The chirality vector of the SWCNT is (20,20), and the GNR is 492 Å in length. The front end of the GNR is marked green. When the simulation time reaches 15 ns, the tail outside the tube is marked blue. (a) Sketch of spirogyra cells whose chloroplasts represent helixes. (b) Concentration distribution profiles of the GNR and SWCNT in the system in the X-direction.

in a helical way, and finally a perfect helix with equal intervals fills up the SWCNT at 15 ns. This helical GNR structure is quite similar to the chloroplast in the spirogyra cell which is shown in panel a below the snapshots in Figure 1. The chloroplast ribbon grows in the helical direction in the spirogyra cell over its entire length,[36] which makes the photosynthesis and the starch storage more efficient. Maybe the coincidence can bring about some enlightenment on the potential applications of this spirogyra-like carbon structure.

Another 10 ns simulation of the GNR tail marked blue outside the tube is carried out to study its evolution. At the beginning, the tail continues moving toward the SWCNT, but the helix in the SWCNT is not possibly pushed out by the tail because the attractive force in the SWCNT is strong enough to trap the GNR helix. The ribbon tail just wraps at the end of the SWCNT instead of forming new segments of the helix. The attractive force from the outer surface makes the tail contact the outer wall of the SWCNT and moves along it helically (at 18 ns). Finally the tail takes the shape of a helix along the outer surface of the SWCNT with an opposite chirality to the SWCNT (at 21 ns).

In panel b of Figure 1, we characterize the geometric parameters of the composite system (omitting the GNR tail outside the tube) by the concentration distribution profiles in the X-direction. From the peak details marked in the inset, the diameter of the helical structure is 19.139 Å, and that of the SWCNT is 25.956 Å. The distance between the helix and the SWCNT is exactly close to 3.5 Å, according well with the stacking distance of the offset face-to-face $\pi-\pi$ stacking interaction[34] which is the distance between the center of one six-membered ring and a plane defined by the opposite six-membered ring, indicating that the $\pi-\pi$ stacking interaction plays a dominant role in the helix-forming process.

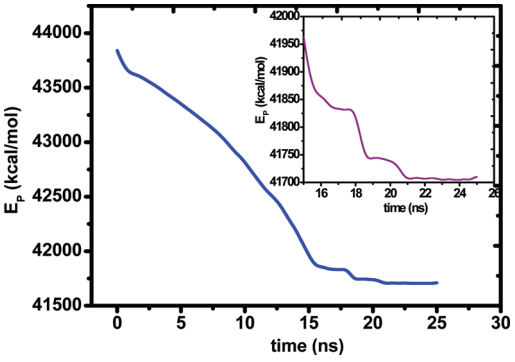

Figure 2. The potential energy as a function of simulation time in the process of helical encapsulation. The inserted graph is the potential energy change during the period from t = 15−25 ns.

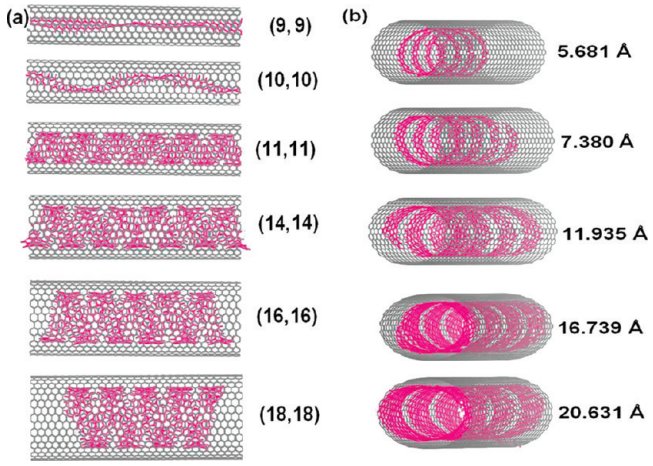

Figure 3. The dependence of the diameter of SWCNT and the width of GNR in the encapsulation process: (a) from top to bottom, the sizes of GNR@SWCNT are GNR(5.681 Å)@SWCNT(9,9), GNR(5.681 Å)@SWCNT(10,10), GNR(7.380 Å)@ SWCNT-(11,11), GNR(7.380 Å)@SWCNT(14,14), GNR(7.380 Å)@SWCNT(16,16) and GNR(7.380 Å)@SWCNT(18,18), respectively; (b) from top to bottom, the sizes of GNR@SWCNT are GNR(5.681 Å)@SWCNT(20,20), GNR(7.380 Å)@SWCNT(20,20), GNR(11.925 Å)@ SWCNT(20,20), GNR(16.735 Å)@SWCNT(20,20), GNR(20.631 Å)@SWCNT(20,20), respectively.

To reveal the energy change of the insertion and helix-forming process, we plot the potential energy curve of the GNR-SWCNT system in Figure 2. The potential energy of the system has decreasing tendency with the simulation time during the first 21 ns, indicating that the encapsulation process of the GNR into the SWCNT is spontaneous. An increase of the contact area between the GNR and SWCNT reduces the systematic potential energy and enhances the stability of the GNR-SWCNT system. At time t = 21 ns, the system reaches the lowest energy, and thereafter the systemic potential energy remains nearly unchanged, suggesting that the whole system is in its equilibrium state.

We have further simulated the dependence of the diameter of SWCNT and the width of GNR in the encapsulation process. From Figure 3, it can be seen that the narrowest graphene nanoribbon with the width of 5.681 Å only contains one string of six-membered rings. When the diameter of the nanotube is smaller than 12 Å (for example, SWCNT (8,8)), the graphene nanoribbon cannot be encapsulated in the nanotube. If the diameter of the nanotube is 12−15 Å (SWCNT (9,9) and SWCNT(10,10)), a GNR helix with large pitch will be formed in the nanotube to reduce the curvature of GNR and keep the whole system stable. When the diameter reaches 15 Å (SWCNT (11,11)), the GNR will produce a perfect helix inside the nanotube just as seen in Figure 3a. To investigate the effect of the width of GNR on the helical encapsulation process, we found that the width of GNR should be less than a threshold value d ($d = D - 2 \times 3.5$ Å) to ensure the insertion of the GNR into the SWCNT (D is the diameter of the carbon nanotube, and 3.5 Å is the distance of the attractive interaction between carbon atoms). Therefore, in the simulation, the valid width range of GNR in the helical encapsulation process is between 5.681 Å and the threshold value d. In addition, if the GNR is a bit wider than the maximum d but can well self-adjust through slight bend or twist, the helical structure will still be formed during the encapsulation process. Owing to the uncontinuity of the size of SWCNT and GNR, it is difficult to figure out an optimized size ratio (SWNT diameter to GNR width) to estimate whether the GNR forms the helical structure. However, when the size of SWCNT and GNR satisfies a fact that the width of the GNR is between 5.681 Å and the threshold value d, and that the diameter of SWCNT is larger than 15 Å, a perfect GNR helical structure will be formed in the carbon nanotube.

In the previous section, we have mainly studied how the one GNR enters the SWCNT. Next, we will clarify how two GNRs encapsulate themselves into the SWCNT. The two GNRs of equal length and width are cut from the adjacent layers in graphite bulk. So one of the GNRs has open edges with dangling σ-orbitals on carbon atoms while the other does not because of the $\pi-\pi$ stacking interaction between two adjacent layers. The two GNRs are placed at three different positions in the SWCNT. In Figure 4a, the two GNRs are separated from each other about 2 nm away at one end of the tube. As the simulation starts, the two GNRs contact each other rapidly due to the $\pi-\pi$ interaction between two layers, while the parts in the SWCNT remain separate. We suggest that the $\pi-\pi$ stacking interaction in the GNR−SWCNT system should be stronger than that in the two layers. It is worth noting that the GNR with open edges tends to more easily form the helical configuration than the other one. The possible cause should be that the open edges reinforce the $\pi-\pi$ stacking interaction through the extra attraction between dangling σ-orbitals on carbon atoms of the open edges and the π electrons in the inner sidewall of the SWCNT.[34] Up to 5 ns, helices arise to both the

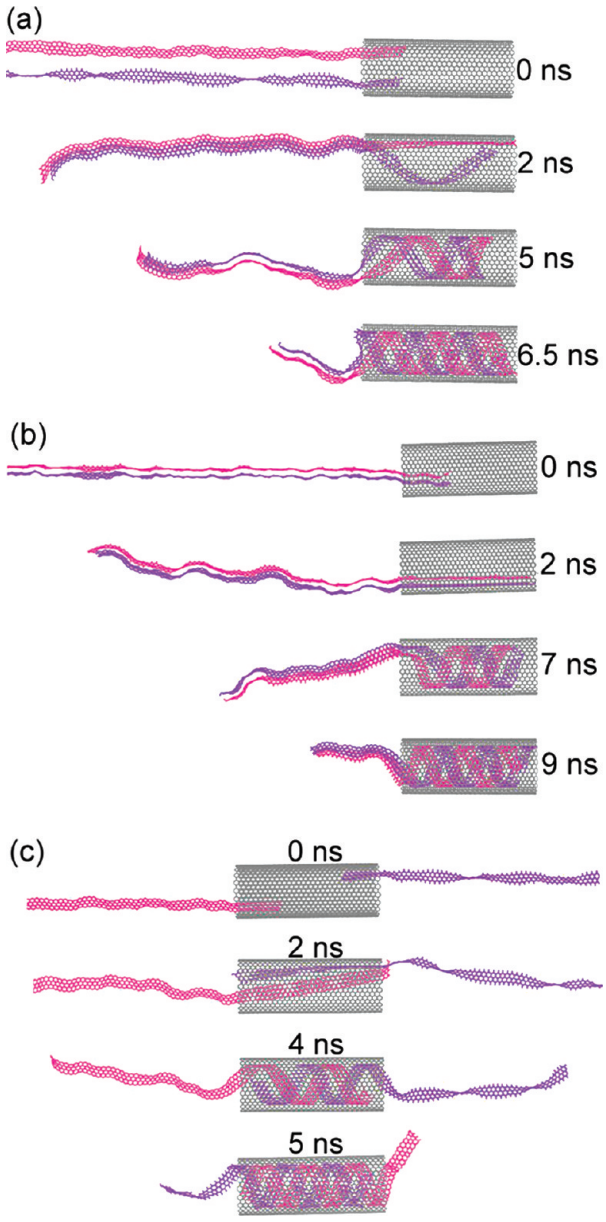

Figure 4. Snapshots of the double-helix of two GNRs inside the SWCNT at three different initial position. The GNRs are both 246 Å in length: (a) insertion of the GNRs into the SWCNT when the two separated graphenes are placed at one end of the SWCNT; (b) insertion of the GNRs into the SWCNT when the two layers contact each other due to the $\pi-\pi$ stacking interaction; (c) insertion of the GNRs into the SWCNT when two separated GNRs are placed at the two ends of the SWCNT, respectively.

ribbons. At the simulation time $t = 6.5$ ns, a clear double helix is formed in the SWCNT. In Figure 4b (see Video 2 in Supporting Information for detailed encapsulation process), the two GNRs are placed at the left end of the SWCNT and initially take on a $\pi-\pi$ stacking. The GNRs enter the SWCNT together until they reach the other end of the tube at the time $t = 2$ ns. As the time progresses, the GNR with open edges is gradually separated from the other one mainly because of the extra attraction between dangling σ-orbitals on carbon atoms of the open edges and the π electrons in the sidewall, and begin to form a double helix. In Figure 4c, the two separated GNRs are placed at the two ends of the SWCNT, respectively. When the simulation starts,

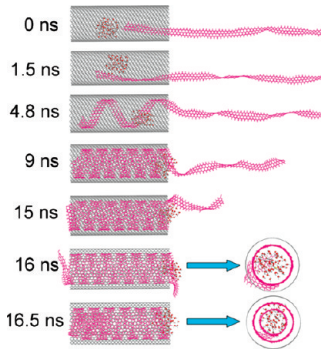

Figure 5. Evolution snapshots of the GNR−SWCNT−water system. The GNR is 492 Å in length. The graphic shows the top views of the snapshots at 16 and 16.5 ns.

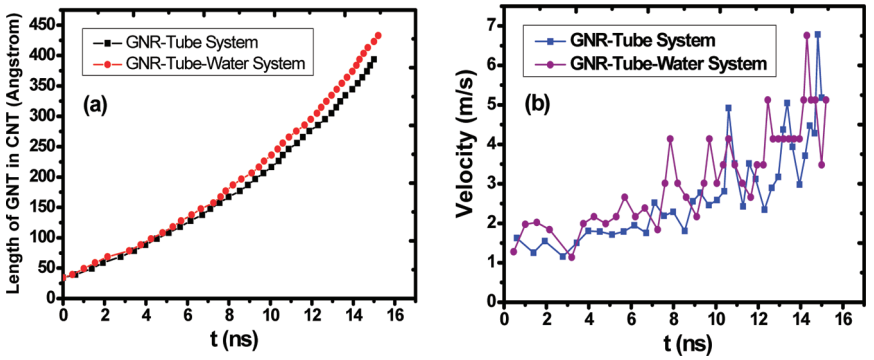

Figure 6. The ribbon length in the SWCNT and the velocity *versus* time in the GNR−SWCNT and the GNR−SWCNT−water system: (a) ribbon length *versus* time; (b) velocity *versus* time.

the two ribbons insert the SWCNT in the reverse directions. Consequently, a reverse double helix appears in the SWCNT, which closely resembles the double-strand DNA. It is worth mentioning that the encapsulation in the reverse directions is more time-saving than that in the same directions due to the increase of the attractive force from the two GNRs.

The above studies mainly focus on the insertion feature of GNRs into the hollow SWCNTs. In this section, we will investigate the insertion characteristic of the GNRs into the SWCNTs initially filled with a small water cluster. To our knowledge, water has some important functions in physical, chemical, and particularly biochemical processes,[37−39] so we introduce a water cluster with 64 molecules in liquid state into the SWCNT to investigate its effects on the insertion and helix-forming process of GNR. It is clear from the snapshots of the first 9 ns in Figure 5 that, with the encapsulation of the GNR into the SWCNT, the water cluster in the SWCNT moves toward the opposite direction owing to the mutual interaction between the GNR and water cluster. The GNR helix is also formed in the SWCNT because of the $\pi-\pi$ stacking interaction. As the simulation progresses, the water cluster reaches the end of the SWCNT and is trapped in the SWCNT owing to the existence of the van der Waals potential well. More interestingly, what is quite different in the case without water cluster (as shown in Figure 1) is that the tail outside of the SWCNT passes through the gap between the water cluster and the tube wall and continues to enter the SWCNT in the helical mode. Finally, the GNR produces a new helix inside the hollow space of the former helix to become a double shell helix at the other end of the SWCNT. Therefore, we suggest that the water cluster should be important to control the conformation of the GNR helix in the SWCNT.

To exploit the effect of the water cluster on the motion of the GNR, Figure 6 shows the curves of ribbon length in the SWCNT and their velocity *versus* time. It is seen that the velocity of the GNR in the GNR−SWCNT−water system is slightly higher than that in the

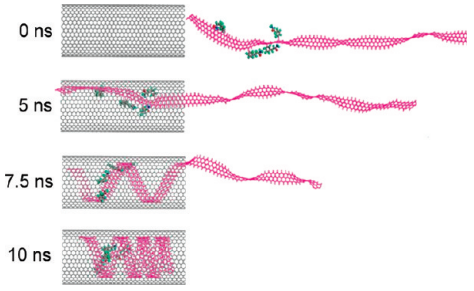

Figure 7. Snapshots of the GNR modified with cinnamamide molecules entering the SWCNT. The length of the GNR is 246 Å.

GNR−SWCNT system because of the attraction from the water cluster. Hence, the water cluster can accelerate GNR to enter into the SWCNTs. Figure 5b shows that both velocities show an increase with time except for some fluctuations, because the mass of the GNR outside the tube keeps decreasing when the attractive force remains virtually unchanged.

The above results arouse our interest in the detection of the properties of GNRs, which can spontaneously fill the SWCNTs to deliver substances into the nanoscale confining space. In this simulation, we chemically attach four cinnamamide molecules, an important substance in biology and medicine,[40−43] to the GNR with a length of 246 Å. Just as shown in Figure 7, the cinnamamide-modified GNR gradually gets into the CNT and forms the helical configuration. The attached molecules have a certain comparatively small impact on the interval between the neighboring segments. Since the distance between the tube and the ribbon and that of the neighboring segments are easily known, we can easily manage the amount of the encapsulated molecules and locate the drug molecules at the specified position in a given SWCNT. Besides the cinnamamide, we can attach other drugs, catalysts, enzymes, *etc.* to the GNR, and let the GNR carry them into the SWCNT. Then we can distribute the drugs or catalysts according to the requirement and make full use of the properties of the confining space in the SWCNT. Hence, the GNR−SWCNT system can be a

promising nanosize biochemical or chemical reaction unit to realize some complex reactions.

CONCLUSION

In this study, it has been observed that the GNR can enter the SWCNT and form helical configuration spontaneously. The van der Waals force traps the GNR in the SWCNT, while the formation of the GNR helix is attributed to the $\pi-\pi$ stacking interaction between the GNR and SWCNT. During the whole encapsulating course, the decline of the potential energy in the GNR−SWCNT system suggests that the helix-forming is a spontaneously phenomenon and the system is increasingly stable during this process. The size of SWCNT and GNR should satisfy some certain conditions. Three simulations on two GNRs placed at different positions in the SWCNT are carried out to investigate the double-helical encapsulation feature of two GNRs. A water cluster may be of great influence to the helical encapsulation process of the GNR into the SWCNT. We has also manifested that the GNR−SWCNT system is of great importance in substance delivery at the nanoscale level.

The above-mentioned discoveries are of great significance in the exploration of the properties of the GNR−SWCNT system. This unique technology may expand the applications of GNR and SWCNT in extensive fields involving medicine, chemistry, biology, and even fuel cells. Maybe the perfect GNR helix maybe used to control the band gap of various GNT-based nanodevices, which will pave the way for the progress of nanoelectronics.

METHODS

The force field of condensed-phase optimized molecular potentials for atomistic simulation studies (Compass)[44] is used to model the atomic interaction. This is an *ab initio* force field that is parametrized and validated using condensed-phase properties in addition to various *ab initio* and empirical data,[45,46] and aims to achieve high accuracy in prediction of the properties of very complex mixtures.[47] Molecular dynamics simulations are performed under an NVT (constant volume and constant temperature dynamics) ensemble at temperature 298 K. The value of the pressure is 0 GPa. The Nose method in the thermostat is applied to control the temperature and generates the correct statistical ensemble. The Verlet algorithm is adopted to integrate the motion of equations of the whole system. The time step is chosen to be 1.0 fs, and data are recorded every 5 ps for further analysis. In the present simulations, the SWCNT (20,20) with the length of 73.79 Å, is fixed as a rigid tube structures. Two sizes of the GNRs are mainly used, which are 492 Å in length and 7.38 Å in width and 246 Å in length and 7.38 Å in width, respectively.

Acknowledgment. We would like to acknowledge the support from the National Natural Science Foundation of China (Grant Nos. 50971081 and 50831003). We also thank the support from the Natural Science Fund for Distinguished Young Scholars of Shandong (JQ200817). This work is also supported by the Natural Science Fund of Shandong Province (ZR2009FM043), by the Ph.D. Dot Programs Foundation of ministry of education of China (No.20090131110025) and by the National Science Fund for Distinguished Young Scholars (No.2009JQ014) from Shandong University. We also thank the support form the Distinguished Postgraduate Innovation Fund (No.10000080398222) from Shandong University and the National Basic Research Program of China (2007CB613901).

Supporting Information Available: Video 1: The insertion and helix-forming process of the GNR into the SWCNT (20,20). Video 2: The double-helix-forming process in which two separated GNRs are placed at the two ends of the SWCNT (20,20). This material is available free of charge *via* the Internet at http://pubs.acs.org.

REFERENCES AND NOTES

1. Matthew, Y. S.; Wang, F.; Huang, L. M.; Chuang, C. C.; Hone, J.; O'Brien, S. P.; Heinz, T. F.; Brus, L. E. Probing Electronic Transitions in Individual Carbon Nanotubes by Rayleigh Scattering. *Science* **2004,** *306*, 1540–1543.
2. Huang, J. Y.; Chen, S.; Wang, Z. Q.; Kempa, K.; Wang, Y. M.; Jo, S. H.; Chen, G. M.; Dresselhaus, S.; Ren, Z. F. Superplastic Carbon Nanotubes. *Nature* **2006,** *439*, 281.
3. Tsang, S. C.; Chen, Y. K.; Harris, P. J. F.; Green, M. L. H. A Simple Chemical Method of Opening and Filling Carbon Nanotubes. *Nature* **1994,** *372*, 159–162.
4. Ajayan, P. M.; Stephan, O.; Redlich, P.; Colliex, C. Carbon Nanotubes as Removable Templates for Metal Oxide Nanocomposites and Nanostructures. *Nature* **1995,** *375*, 564–567.
5. Choi, W. Y.; Kang, J. W.; Hwang, H. J. Structures of Ultrathin Copper Nanowires Encapsulated in Carbon Nanotubes. *Phys. Rev. B* **2003,** *68*, 193405.
6. Ajayan, P. M.; Colliex, C.; Lambert, J. M.; Bernier, P.; Barbedette, L.; Tencé, M.; Stephan, O. Growth of Manganese Filled Carbon Nanofibers in the Vapor Phase. *Phys. Rev. Lett.* **1994,** *72*, 1722–1725.
7. Setlur, A. A.; Lauerhaas, J. M.; Dai, J. Y.; Chang, R. P. H. A Method for Synthesizing Large Quantities of Carbon Nanotubes and Encapsulated Copper Nanowires. *Appl. Phys. Lett.* **1996,** *69*, 345–347.
8. Shao, J. L.; Yang, C.; Zhu, X. L.; Lu, X. H. Melting and Freezing of Au Nanoparticles Confined in Armchair Single-Walled Carbon Nanotubes. *J. Phys. Chem. C* **2010,** *114*, 2896–2902.
9. Wang, L.; Zhang, H. W.; Zhang, Z. Q.; Zheng, Y. G.; Wang, J. B. Buckling Behaviors of Single-Walled Carbon Nanotubes Filled with Metal Atoms. *Appl. Phys. Lett.* **2007,** *91*, 051122.
10. Cicero, G.; Grossman, J. C.; Schwegler, E.; Gygi, F.; Galli, G. Water Confined in Nanotubes and between Graphene Sheets: A First Principle Study. *J. Am. Chem. Soc.* **2008,** *130*, 1871–1878.
11. Striolo, A. The Mechanism of Water Diffusion in Narrow Carbon Nanotubes. *Nano Lett.* **2006,** *6*, 633–639.
12. Hummer, G.; Rasaiah, J. C.; Noworyta, J. P. Water Conduction through the Hydrophobic Channel of a Carbon Nanotube. *Nature* **2001,** *414*, 188–190.
13. Vidossich, P.; Cascella, M.; Carloni, P. Dynamics and Energetics of Water Permeation through the Aquaporin Channel. *Proteins* **2004,** *55*, 924–931.
14. Bai, J.; Wang, J.; Zeng, X. C. Multiwalled Ice Helixes and Ice Nanotubes. *Proc. Natl. Acad. Sci. U.S.A.* **2006,** *103*, 19664–19667.
15. Gao, H.; Kong, Y.; Cui, D.; Ozkan, C. S. Spontaneous Insertion of DNA Oligonucleotides into Carbon Nanotubes. *Nano Lett.* **2003,** *3*, 471–473.
16. Zou, J.; Liang, W. T.; Zhang, S. L. Coarse-Grained Molecular Dynamics Modeling of DNA−Carbon Nanotube Complexes. *Int. J. Numer. Methods Eng.* **2010,** *83*, 968–985.
17. Wang, Z. Y.; Li, H.; Liu, Z.; Shi, Z. J.; Lu, J; Suenaga, K.; Joung, S. J.; Okazaki, T.; Gu, Z. N.; Zhou, J.; *et al.* Mixed

Low-Dimensional Nanomaterial: 2D Ultranarrow MoS_2 Inorganic Nanoribbons Encapsulated in Quasi-1D Carbon Nanotube. *J. Am. Chem. Soc.* **2010,** *132*, 13840–13847.
18. Okada, S.; Saito, S.; Oshiyama, A. Energetics and Electronic Structures of Encapsulated C_{60} in a Carbon Nanotube. *Phys. Rev. Lett.* **2001,** *86*, 3835–3838.
19. Warner, J. H.; Wilson, M. Elastic Distortions of Carbon Nanotubes Induced by Chiral Fullerene Chains. *ACS Nano* **2010,** *4*, 4011–4016.
20. Frank, O.; Tsoukleri, G.; Parthenios, J.; Papagelis, K.; Riaz, I.; Jalil, R.; Novoselov, K. S.; Galiotis, C. Compression Behavior of Single-Layer Graphenes. *ACS Nano* **2010,** *4*, 3131–3138.
21. Seol, J. H.; Jo, I.; Moore, A. L.; Lindsay, L; Aitken, Z. H.; Pettes, M. T.; Li, X.; Yao, Z.; Huang, R.; Broido, D.; *et al.* Two-Dimensional Phonon Transport in Supported Graphene. *Science* **2010,** *328*, 213–216.
22. Lee, C.; Wei, X.; Kysar, J. W.; Hone, J. Measurement of the Elastic Properties and Intrinsic Strength of Monolayer Graphene. *Science* **2008,** *321*, 385–388.
23. Xu, Z. P.; Buehler, M. J. Geometry Controls Conformation of Graphene Sheets: Membranes, Ribbons, and Scrolls. *ACS Nano* **2010,** *4*, 3869–3876.
24. Ezawa, M. Peculiar Width Dependence of the Electronic Properties of Carbon Nanoribbons. *Phys. Rev. B* **2006,** *73*, 045432.
25. Son, Y. W.; Cohen, M. L.; Louie, S. G. Energy Gaps in Graphene Nanoribbons. *Phys. Rev. Lett.* **2006,** *97*, 216803.
26. Son, Y. W.; Cohen, M. L.; Louie, S. G. Half-Metallic Graphene Nanoribbons. *Nature* **2006,** *444*, 347–349.
27. Hod, O.; Barone, V.; Peralta, J. E.; Scuseria, G. E. Enhanced Half-Metallicity in Edge-Oxidized Zigzag Graphene Nanoribbons. *Nano Lett.* **2007,** *7*, 2295–2299.
28. Dutta, S.; Manna, A. K.; Pati, S. K. Intrinsic Half-Metallicity in Modified Graphene Nanoribbons. *Phys. Rev. Lett.* **2009,** *102*, 096601.
29. Gunlycke, D.; Li, J.; Mintmire, J. W.; White, C. T. Altering Low-Bias Transport in Zigzag-Edge Graphene Nanostrips with Edge Chemistry. *Appl. Phys. Lett.* **2007,** *91*, 112108.
30. Yang, X. Y.; Zhang, Z. Y.; Liu, Z. F.; Ma, Y. F.; Huang, Y.; Chen, Y. S. High Efficiency Loading and Controlled Release of Doxorubicin Hydrochloride on Graphene Oxide. *J. Phys. Chem. C* **2008,** *112*, 17554–17558.
31. Liu, Z.; Robinson, J. T.; Sun, X. M.; Dai, H. J. PEGylated Nanographene Oxide for Delivery of Water-Insoluble Cancer Drugs. *J. Am. Chem. Soc.* **2008,** *130*, 10876–10877.
32. Bets, K. V.; Jacobson, B. I. Spontaneous Twist and Intrinsic Instabilities of Pristine Graphene Nanoribbons. *Nano Res.* **2009,** *2*, 161–166.
33. Fasolino, A.; Los, J. H.; Katsnelson, M. I. Intrinsic Ripples in Graphene. *Nat. Mater.* **2007,** *6*, 858–861.
34. Główbka, M. L.; Martynowski, D.; Kozłowska, K. Stacking of Six-Membered Aromatic Rings in Crystals. *J. Mol. Struct.* **1999,** *474*, 81–89.
35. Snir, Y.; Kamien, R. D. Entropically Driven Helix Formation. *Science* **2005,** *307*, 1067.
36. Ohiwa, T. Observations on Chloroplast Growth and Pyrenoid Formation in *Spirogyra*. A Study by Means of Uncoiled Picture of Chloroplast. *J. Plant Res.* **1976,** *89*, 259–266.
37. Feng, G.; Qiao, R.; Huang, J. S.; Sumpter, B. G.; Mwunier, V. Ion Distribution in Electrified Micropores and Its Role in the Anomalous Enhancement of Capacitance. *ACS Nano* **2010,** *4*, 2382–2390.
38. Wu, C. F. Cooperative Behavior of Poly(vinyl alcohol) and Water as Revealed by Molecular Dynamics Simulations. *Polymer* **2010,** *51*, 4452–4460.
39. Argyris, D.; Cole, D. R.; Striolo, A. Ion-Specific Effects under Confinement: The Role of Interfacial Water. *ACS Nano* **2010,** *4*, 2035–2042.
40. Jiang, X. F.; Zhen, Y. S. Cinnamamide, an Antitumor Agent with Low Cytotoxicity Acting on Matrix Metalloproteinase. *Anticancer Drugs* **2000,** *11*, 49–54.
41. Villani, F. J.; Lang, J.; Papa, D. Amides of Ethylenediamines. II. Substituted Cinnamides as Local Anesthetic Agents. *J. Am. Chem. Soc.* **1954,** *76*, 87–88.
42. Moffet, R. B. Central Nervous System Depressants. VI. Polymethoxyphenyl Esters and Amides. *J. Med. Chem.* **1964,** *7*, 319–325.
43. Gill, E. L.; Feare, C. J.; Cowan, D. P.; Fox, S. M.; Bishop, J. D.; Langton, S. D.; Watkins, R. W.; Gurney, J. E. Cinnamamide Modifies Foraging Behaviors of Free-Living Birds. *J. Wildl. Manage.* **1998,** *72*, 872–884.
44. Sun, H. COMPASS: An *Ab Initio* Force-Field Optimized for Condensed-Phase Applications Overview with Details on Alkane and Benzene Compounds. *J. Phys. Chem. B* **1998,** *102*, 7338–7364.
45. Wang, Q. Atomic Transportation *via* Carbon Nanotubes. *Nano Lett.* **2009,** *9*, 245–249.
46. Wang, Q. Transportation of Hydrogen Molecules Using Carbon Nanotubes in Torsion. *Carbon* **2009,** *47*, 1870–1873.
47. Bunte, S. W.; Sun, H. Molecular Modeling of Energetic Materials: The Parameterization and Validation of Nitrate Esters in the COMPASS Force Field. *J. Phys. Chem. B* **2000,** *104*, 2477–2489.